The effect of CO_2 and H_2O on the kinetics of NO reduction by CH_4 over Sr-promoted La_2O_3

Todd J. Toops, Arden B. Walters, and M. Albert Vannice *

Department of Chemical Engineering, Pennsylvania State University, University Park, PA 16802-4400, USA

Received 11 January 2001; accepted 4 April 2002

The influence of CO_2 and H_2O on the activity of 4% Sr-La_2O_3 mimics that observed with pure La_2O_3, and a reversible inhibition of the rate is observed. CO_2 causes a greater effect, with decreases in rate of about 65% with O_2 present and 90% in its absence, while with H_2O in the feed, the rate decreased around 35–40% with O_2 present or absent. The influence of these two reaction products on kinetic behavior can be described by assuming competitive adsorption on the surface, incorporating adsorbed CO_2 and H_2O in the site balance, and using rate expressions previously proposed for this reaction over Sr-promoted La_2O_3. In the absence of O_2, the rate expression is

$$r_{N_2} = \frac{k' P_{NO} P_{CH_4}}{(1 + K_{NO} P_{NO} + K_{CH_4} P_{CH_4} + K_{CO_2} P_{CO_2} + K_{H_2O} P_{H_2O})^2},$$

which yields a good fit to the experimental data and gives optimized equilibrium adsorption constants that demonstrate thermodynamic consistency. With O_2 in the feed, nondifferential changes in reactant concentrations through the reactor bed were accounted for by assuming integral reactor behavior and simultaneously considering both CH_4 combustion and CH_4 reduction of NO, which provided the following rate law for total CH_4 disappearance:

$$(r_{CH_4})_T = \frac{k'_{com} P_{CH_4} P_{O_2}^{0.5} + k'_{NO} P_{NO} P_{CH_4} P_{O_2}^{0.5}}{(1 + K_{NO} P_{NO} + K_{CH_4} P_{CH_4} + K_{O_2}^{0.5} P_{O_2}^{0.5} + K_{CO_2} P_{CO_2} + K_{H_2O} P_{H_2O})^2}.$$

The second term of this expression represents N_2 formation, and it again fit the experimental data well. The fitting constants in the denominator, which correspond to equilibrium adsorption constants, were not only thermodynamically consistent but also provided entropies and enthalpies of adsorption that were similar to values obtained with other La_2O_3-based catalysts. Apparent activation energies typically ranged from 23 to 28 kcal/mol with O_2 absent and 31–36 kcal/mol with O_2 in the feed. With CO_2 in the feed, but no O_2, the activation energy for the formation of a methyl group *via* interaction of CH_4 with adsorbed NO was determined to be 35 kcal/mol.

KEY WORDS: NO reduction; SCR kinetics; CH_4; Sr-promoted La_2O_3; CO_2; H_2O.

1. Introduction

The promoting effect of Sr on La_2O_3 catalysts has been demonstrated in both methane oxidative coupling (MOC) [1–3] and NO reduction [4–6] reactions. Evidence indicates that Sr promotes the formation of oxygen vacancies in the La_2O_3 lattice, particularly at the surface, thus generating more active sites [5,7–9]. In MOC reactions, CO_2 helps stabilize an active phase in Sr-La_2O_3 [10], and H_2O has also been found to have a beneficial effect [11]; however, no studies have examined the effects of these two components on NO reduction over Sr-promoted La_2O_3. Thus, the present investigation addresses NO reduction by CH_4 over a 4% Sr-La_2O_3 catalyst between 773 and 973 K in the presence and absence of O_2 because it had been previously determined that this Sr loading optimized the performance of this system [4–6]. The standard concentrations of these two flue components, i.e., 9% CO_2 and 2% H_2O, were the same as in another study, but SO_2 was not examined because of its poisoning effect on La_2O_3 [12]. Reaction orders were determined along with specific activities and activation energies, and a reaction mechanism previously proposed was modified to account for the effects of CO_2 and H_2O in either the absence or the presence of O_2. The equilibrium adsorption constants for CH_4, NO, O_2, CO_2, and H_2O obtained from the optimized fitting constants in the rate expressions were further evaluated to verify thermodynamic consistency. In this study the catalyst was also characterized before and after kinetic experimentation using X-ray diffraction, BET surface area measurements, and NO chemisorption.

2. Experimental

The Sr-promoted La_2O_3 catalyst was prepared by dissolving $Sr(NO_3)_2$ (Aldrich, 99.995%) in distilled, deionized water in the appropriate quantity, slowly adding this solution to La_2O_3, and then heating this mixture

* To whom correspondence should be addressed.
E-mail: mavche@engr.psu.edu

1011-372X/02/0900-0045

until only a paste remained. To provide homogeneity in the catalyst, fresh water was added to the paste followed by drying; this last cycle was repeated two more times, then the catalyst was dried overnight in air at 400 K. The catalyst was ground into a powder and calcined for 10 h at 1023 K under 50 cm^3 (STP)/min of O_2 (MG Ind., 99.999%). The BET surface area, total and reversible NO uptakes, and the bulk crystal structure of the catalyst were determined before and after reaction.

Initial surface areas were determined using the approach described elsewhere [13], while the surface area of a used sample was obtained by transferring the quartz adsorption cell with a catalyst sample to the reactor system, ramping from 300 to 973 K at 11 K/min and holding there for 1 h while flowing a mixture of 10% O_2 in He at 20 cm^3 (STP)/min. The catalyst was then maintained at 973 K overnight under standard reaction conditions, purged with 50 cm^3 (STP)/min He for 30 min, closed off, quenched to 300 K, transferred to the adsorption system, and evacuated. Physical adsorption measurements were then conducted as described previously [13].

Chemisorption of NO was determined in the same system as that used for the BET experiments, and the same general procedure was followed. For fresh samples, the standard pretreatment was used, i.e., 20 cm^3 (STP)/min of 10% O_2 in He at 973 K for 1 h, with an 11 K/min ramp from ambient temperature. The catalyst was then evacuated for 30 min, cooled to room temperature, and NO chemisorption was measured at 300 K. The sample was then evacuated for 1 h and the sequence was repeated to generate the reversible adsorption isotherm. The difference between the two isotherms yielded the irreversibly chemisorbed NO. To determine NO chemisorption after a kinetic experiment, the procedure followed was that previously described for surface area determination of a used catalyst.

X-ray diffraction (XRD) patterns were used to monitor phase changes in the La_2O_3, and they were obtained *ex situ* utilizing a Philips MPD X-ray diffractometer with Cu K_α radiation following a procedure described earlier [13]. For analysis of post-reaction catalysts, the reactor was cooled in 20 cm^3 (STP) He/min and the catalyst was transferred to a desiccator prior to analysis.

The kinetic studies were performed in a reactor system similar to that described previously [14], except that a P-E Sigma 3 gas chromatograph (GC) was combined with a P-E Nelson 1020 integrator and a chemiluminescence NO_x analyzer (Thermo Environmental Instr. Inc., Model 42H) was installed downstream from the GC to differentiate between NO and NO_2 in the effluent. The GC temperature program provided good separation of N_2, O_2, NO, CO, CH_4, CO_2, N_2O and H_2O, although the last peak was not quantifiable [12]. Unless otherwise specified, experiments in the presence of O_2 were performed with 25 mg of catalyst and a feed containing 1.4% NO, 0.35% CH_4 and 1.0% O_2 in He flowing at 45 cm^3 (STP)/min. In the absence of O_2, the concentrations were not changed, but 75 mg catalyst was used with a lower total flow rate (25 cm^3 (STP)/min) because the activity was lower. The effects of CO_2 or H_2O were studied separately using standard concentrations of 9.0% or 2.0% in He, respectively. Distilled, deionized water was introduced to the reactor system *via* He flowing through a saturator placed in a Neslab GP-100 constant temperature bath. All stainless steel tubing leading to and from the reactor was heated at 323 K to avoid water condensation. The gas mixtures used in the experiments were 4.03% NO in He, 9.80% O_2 in He and 1.0% CH_4 in He, and they were prepared with gases from MG Ind. (99.999% except for NO, which was 99.0+%). The CO_2 was also from MG Ind. (99.995%).

The standard catalyst pretreatment in the kinetic experiments involved heating for 1 h at 973 K under 20 cm^3 (STP)/min of 10% O_2 in He. The feed mixture was flowed for at least 30 min before any data were recorded. NO reduction with CH_4 was studied between 773 and 973 K, and a descending then an ascending temperature sequence was used to check for any deactivation; other details are provided elsewhere [12]. Activity *versus* time on stream (TOS) was also monitored to determine the transient effects of CO_2 or H_2O in the feed stream on NO reduction.

Activity dependencies on H_2O and CO_2 partial pressures were determined at three or four temperatures between 873 and 973 K by varying the inlet partial pressure of one reactant while keeping all other reactant concentrations and the total flow rate constant. The standard feed concentrations were 11 Torr NO (1.4%), 2.7 Torr CH_4 (0.35%) and 7.6 Torr O_2 (1.0%) in He. NO was varied from 1.9 to 15 Torr (0.25–2.2%), CH_4 from 0.38 to 3.4 Torr (0.05–0.55%), O_2 from 1.9 to 22 Torr (0.35–1.8%), CO_2 from 8 to 130 Torr (1.0–17%), and H_2O from 2.3 to 22 Torr (0.3–3.0%). Generally, a new catalyst was used for each test, which caused minor variations in the rates; however, all pressure-dependency rates were normalized to the Arrhenius plot at standard conditions to eliminate this complication during the data-fitting optimization.

3. Results

As with La_2O_3, CO_2 induced a reversible inhibition of NO reduction by CH_4 over 4% $Sr\text{-}La_2O_3$ in either the absence or the presence of O_2, as depicted by the Arrhenius plots in figure 1. Each gas hourly space velocity (GHSV) was calculated using an approximate catalyst density of 1.45 g/cm^3. Apparent activation energies were determined in the differential regime, depicted by solid lines in the Arrhenius plots, where all reactant conversions were less than 20%. Rates and specific activities at 873 and 973 K are reported in table 1. The

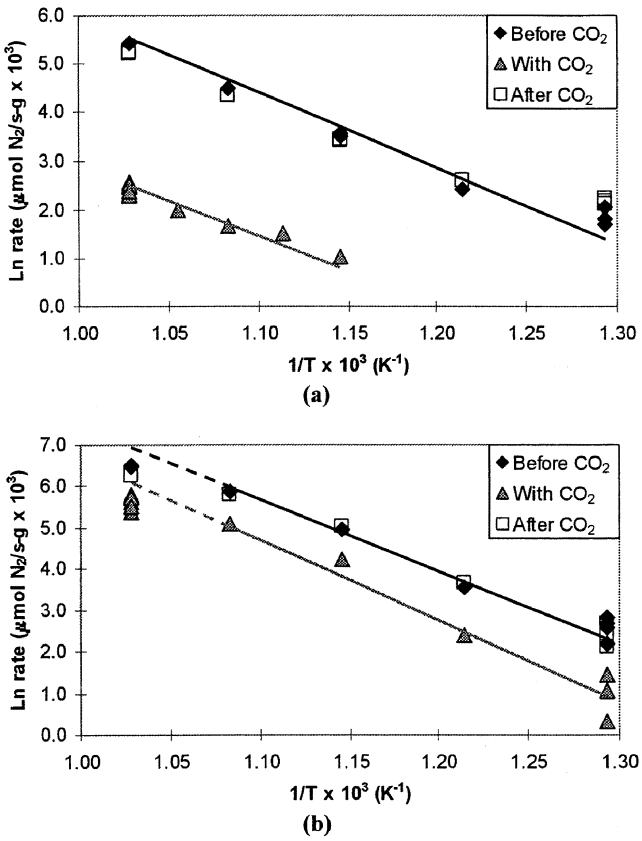

Figure 1. Arrhenius plots illustrating the effect of CO_2 on NO reduction by CH_4 over 4% $Sr\text{-}La_2O_3$ in (a) the absence of O_2 and (b) in the presence of O_2. Reactor conditions: 1.4% NO, 0.35% CH_4, 0 or 1.0% O_2, 0 or 9.0% CO_2, balance He; GHSV = 28 000 h^{-1} in the absence of O_2 and 130 000,h^{-1} in the presence of O_2.

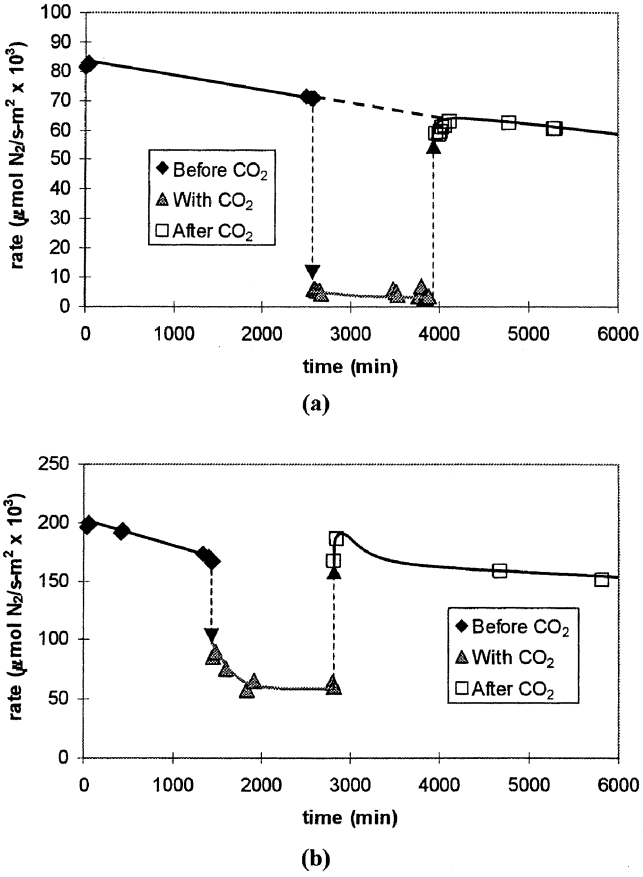

Figure 2. Activity for NO reduction by CH_4 *versus* time on stream in the presence of CO_2 in (a) the absence of O_2 and (b) the presence of O_2. Reactor conditions: 1.4% NO, 0.35% CH_4, 0 or 1.0% O_2, and 0 or 9.0% CO_2, balance He; GHSV = 30 000 h^{-1} in the absence of O_2 and 140 000 h^{-1} in the presence of O_2.

Table 1
Apparent activation energies for 4% $Sr\text{-}La_2O_3$

	Rate (μmol N_2/s g × 10^3)		Specific activity (μmol N_2/s m^2 × 10^3)		E_a (kcal/mol)
	873 K	973 K	873 K	973 K	
9% CO_2 study					
O_2 absent					
Before CO_2	34	230	11	72	27 ± 2
With CO_2	2.8	12	0.89	3.9	23 ± 3
After CO_2	30	190	9.6	61	23 ± 2
O_2 present					
Before CO_2	143	660	41	190	31 ± 5
With CO_2	65	300	19	84	35 ± 4
After CO_2	150	530	44	150	33 ± 6
2% H_2O study					
O_2 absent					
Before H_2O	39	230	12	73	27 ± 2
With H_2O	22	150	7.0	46	27 ± 2
After H_2O	32	230	10	73	28 ± 2
O_2 present					
Before H_2O	172	730	55	230	43 ± 9
With H_2O	55	310	17	99	36 ± 9
After H_2O	150	530	46	170	35 ± 4

Reactor conditions: 1.4% NO, 0.35% CH_4, 0 or 1.0% O_2, 0 or 9.0% CO_2, 0 or 2% H_2O, balance He; GHSV = 30 000 h^{-1} in the absence of O_2 and 130 000 h^{-1} in the presence of O_2.

effect of CO_2 was also examined by monitoring activity *versus* time on stream, as shown in figure 2, to determine if the inhibition was transient. A similar reversible effect was observed when the influence of H_2O on NO reduction was examined, as depicted by the Arrhenius plots in figure 3. The kinetic results are also reported in table 1 for each set of conditions, while a portrayal of activity *versus* time on stream is given in figure 4. In each case N_2 was the predominant product during NO reduction, with N_2O formation comprising less than 10% of the total NO reduction rate.

Reaction orders were determined in the absence of oxygen at four temperatures between 898 and 973 K following the procedure described earlier [13], and they are listed in table 2, while the kinetic data are displayed in figure 5 for CO_2 and figure 6 for H_2O. Although NO conversions were always below 20%, direct combustion of CH_4 by O_2 was significant; thus integral reactor behavior was assumed in the analysis of rate data. Due to this complication, the reaction orders obtained from a power-rate law and listed in table 2 should be considered to be approximate. The data for the partial pressure dependencies with O_2 and either CO_2 or H_2O are displayed in figures 7 and 8, respectively.

The XRD spectra indicated the influence of CO_2 or H_2O on the phases observable in the promoted La_2O_3.

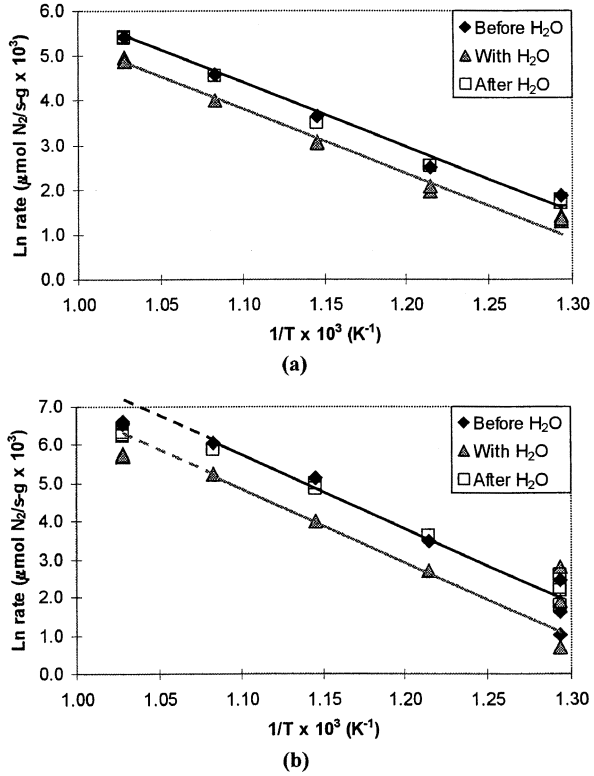

Figure 3. Arrhenius plots illustrating the effect of H_2O on NO reduction by CH_4 over 4% $Sr\text{-}La_2O_3$ in (a) the absence of O_2 and (b) the presence of O_2. Reactor conditions: 1.4% NO, 0.35% CH_4, 0 or 1.0% O_2, 0 or 2.0% H_2O, balance He; GHSV = 30 000 h^{-1} in the absence of O_2 and 140 000 h^{-1} in the presence of O_2.

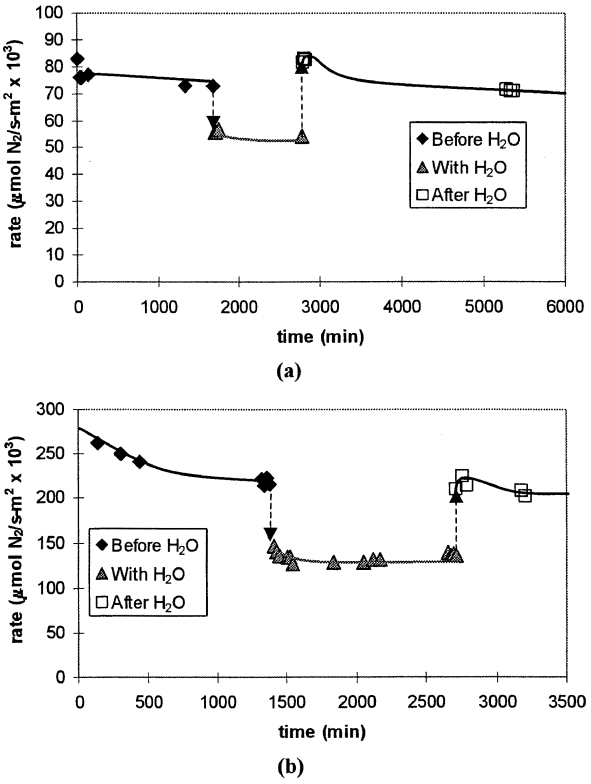

Figure 4. Activity for NO reduction by CH_4 *versus* time on stream in the presence of H_2O in (a) the absence of O_2 and (b) the presence of O_2. Reactor conditions: 1.4% NO, 0.35% CH_4, 0 or 1.0% O_2, and 0 or 2.0% H_2O, balance He; GHSV = 30 000 h^{-1} in the absence of O_2 and 140 000 h^{-1} in the presence of O_2.

Table 2
Reaction orders for the reduction of NO by CH_4 over 4% $Sr\text{-}La_2O_3$

	NO	CH_4	O_2	CO_2	H_2O
CO_2 study					
O_2 absent					
973 K	0.56	0.08	–	−0.21	–
960 K	0.45	0.21	–	−0.20	–
948 K	0.54	0.23	–	−0.17	–
923 K	0.51	0.25	–	−0.14	–
O_2 present					
923 K	0.74	0.51	0.25	−0.11	–
908 K	0.74	0.48	0.17	−0.05	–
893 K	0.76	0.64	−0.19	−0.04	–
873 K	0.66	0.73	−0.33	−0.17	–
H_2O study					
O_2 absent					
973 K	0.97	0.32	–	–	−0.23
948 K	0.89	0.28	–	–	−0.29
923 K	0.98	0.26	–	–	−0.39
898 K	1.07	0.21	–	–	−0.40
O_2 present					
923 K	0.41	0.74	−0.03	–	−0.17
908 K	0.41	0.73	−0.08	–	−0.33
893 K	0.45	0.75	−0.16	–	−0.20
873 K	0.41	0.80	−0.02	–	−0.34

Standard reactor conditions: 1.4% NO, 0.35% CH_4, 0 or 1.0% O_2, 0 or 9.0% CO_2, 0 or 2.0% H_2O, balance He; GHSV = 30 000 h^{-1} in the absence of O_2 and 140 000 h^{-1} in the presence of O_2.

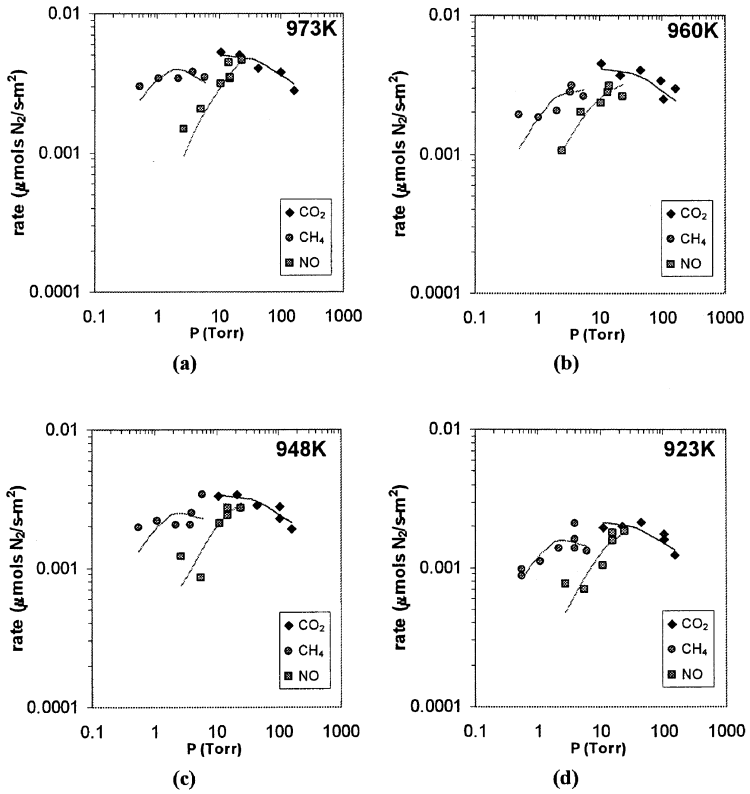

Figure 5. Partial pressure dependencies for NO reduction by CH_4 with CO_2 but no O_2 in the feed at (a) 973 K, (b) 960 K, (c) 948 K and (d) 923 K. Symbols represent experimental data, and the rate expression given by equation (8) is represented by lines. Standard reactor conditions: 1.4% NO, 0.35% CH_4, and 9% CO_2, balance He; GHSV = 30 000 h^{-1}.

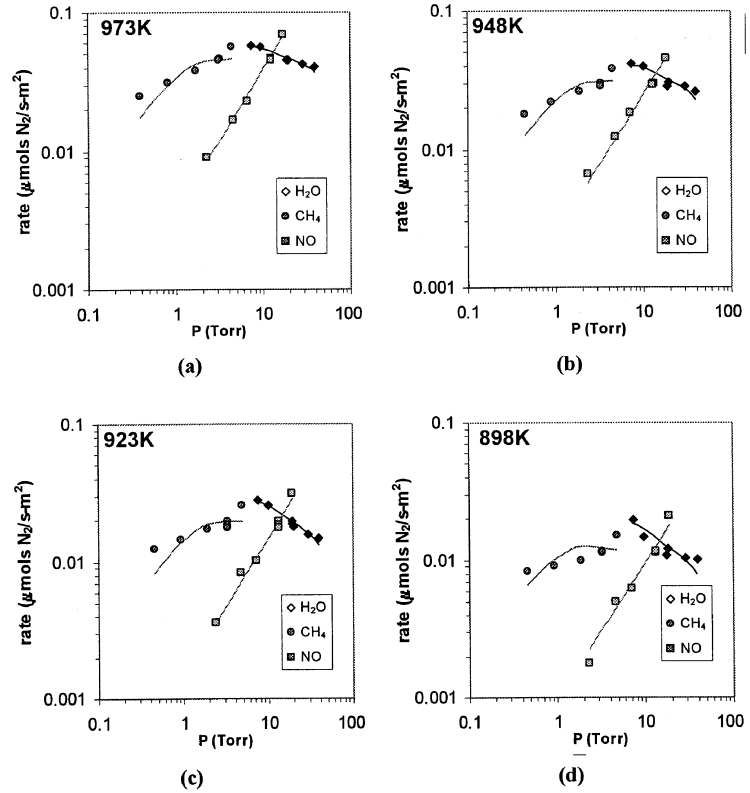

Figure 6. Partial pressure dependencies for NO reduction by CH_4 with H_2O but no O_2 in the feed at (a) 973 K, (b) 948 K, (c) 923 K and (d) 898 K. Symbols represent experimental data, and the rate expression given by equation (8) is represented by lines. Standard reactor conditions: 1.4% NO, 0.35% CH_4, and 2.0% H_2O, balance He; GHSV = 30 000 h^{-1}.

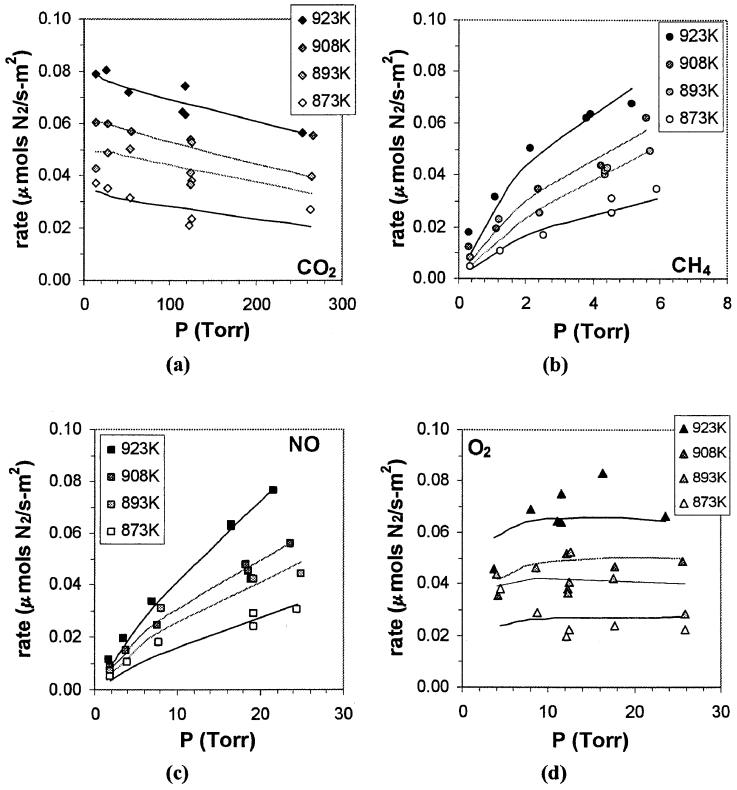

Figure 7. Partial pressure dependencies for NO reduction by CH_4 with CO_2 and O_2 in the feed between 873 and 923 K for (a) CO_2, (b) CH_4, (c) NO and (d) O_2. Symbols represent experimental data, and the rate expression given by equation (19) is represented by lines. Standard reactor conditions: 1.4% NO, 0.35% CH_4, 1.0% O_2 and 9% CO_2, balance He; GHSV = 140 000,h^{-1}.

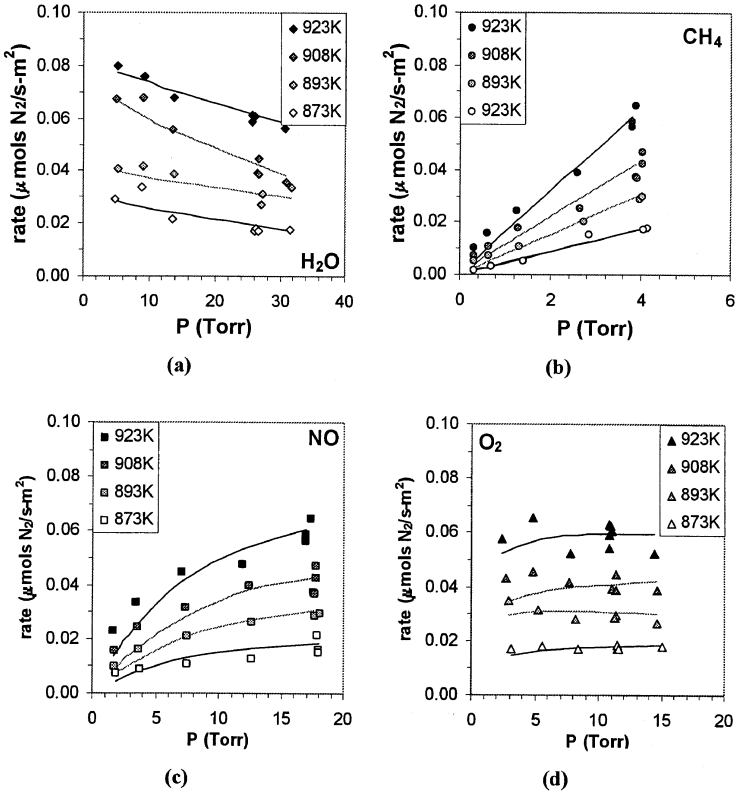

Figure 8. Partial pressure dependencies for NO reduction by CH_4 with H_2O and O_2 in the feed between 873 and 948 K for: (a) H_2O, (b) CH_4, (c) NO and (d) O_2. Symbols represent experimental data, and the rate expression given by equation (19) is represented by lines. Standard reactor conditions: 1.4% NO, 0.35% CH_4, 1.0% O_2 and 2.0% H_2O, balance He; GHSV = 141 000 h^{-1}.

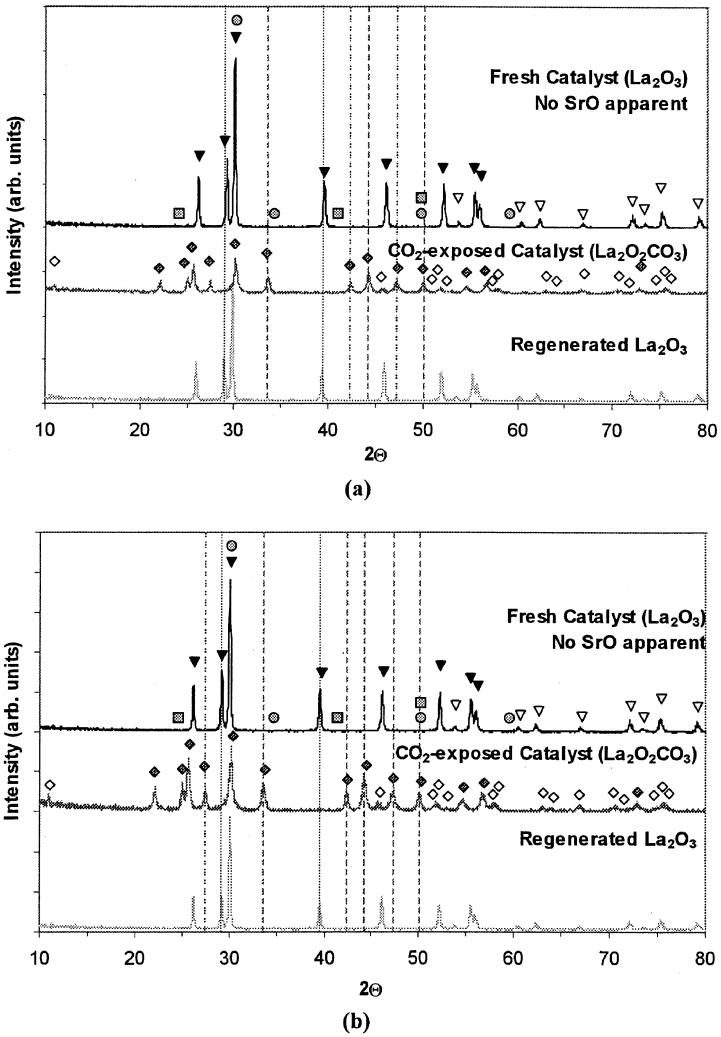

Figure 9. XRD patterns characterizing the effects of CO_2 on the phases present in 4% Sr-La_2O_3 in (a) the absence of O_2 and (b) the presence of O_2. Lines represent unique peaks for La_2O_3 (·····) and $La_2O_2CO_3$ (– – – –). Symbols represent characteristic peaks for La_2O_3 (▼, ▽), II-$La_2O_2CO_3$ (◆, ◇), Sr (●), and SrO (■). Filled symbols represent principal peaks.

After reaction with CO_2 in the feed, a bulk transformation from La_2O_3 to an oxycarbonate (II-$La_2O_2CO_3$) phase had occurred, as shown by the XRD patterns in figure 9. This phase disappeared when CO_2 was removed from the reactor feed stream, and the catalyst reverted to the La_2O_3 phase in either the presence or absence of O_2 in the feed. This same behavior was observed with unpromoted La_2O_3 [12]. No bulk-phase transformation was observed with H_2O in the feed, which is consistent with earlier observations [12,15,16].

The results from the XRD study suggested that the surface area or the type of NO adsorption sites may also change during reaction, so these two parameters were determined after operation at each of the reaction conditions of interest following a specific procedure [12]. The NO chemisorption isotherms at 300 K are shown in figures 10 and 11 after exposure to CO_2 and H_2O, respectively, and table 3 lists the results of these adsorption experiments.

4. Discussion

Similarly to unpromoted La_2O_3 [12], 4% Sr-La_2O_3 maintained activity for NO reduction by methane when CO_2 or H_2O was included in the feed, but rate inhibition did occur. The latter two components are of considerable interest because they are present in any practical NO reduction feed stream, and steam has already been found to cause irreversible deactivation of a promising catalyst [17–19]. This deactivation has attracted attention, and NO reduction studies have been conducted on oxide-based catalysts with H_2O in the feed stream [19–29]. These results are compared to those for Sr-La_2O_3 in table 4, with respect to rate and, whenever possible, on a turnover frequency or specific activity basis also. In this study TOFs were determined by dividing the rate of N_2 production by the number of sites capable of irreversible NO adsorption (μmol NO/g) at 300 K, whereas other rates in table 4 were normalized to the

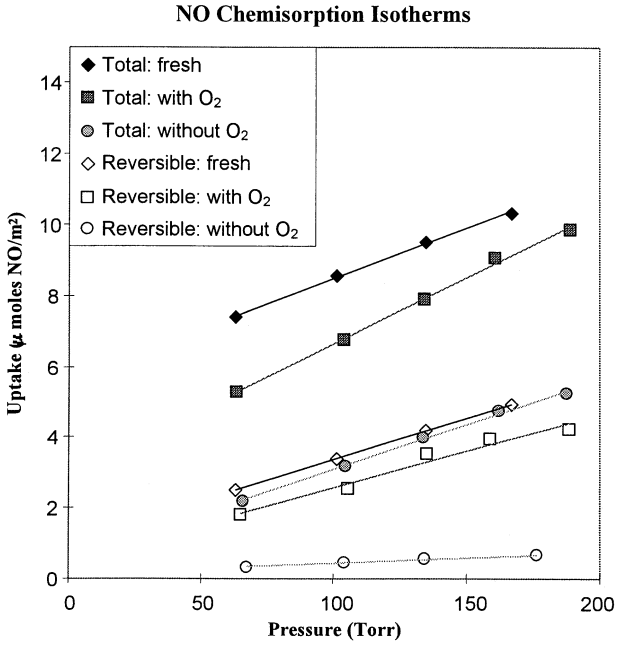

Figure 10. Effect of CO_2 in feed stream on NO chemisorption at 300K after quenching. Reaction conditions: 973 K and either GHSV = 4600 h^{-1} for 10% O_2/He pretreatment (fresh) (◆, ◇) and 1.4% NO, 0.35% CH_4, 0% O_2, 9% CO_2, balance He (●, ○), or GHSV = 8300 h^{-1} for 1.4% NO, 0.35% CH_4, 1% O_2, 9% CO_2, balance He (■, □).

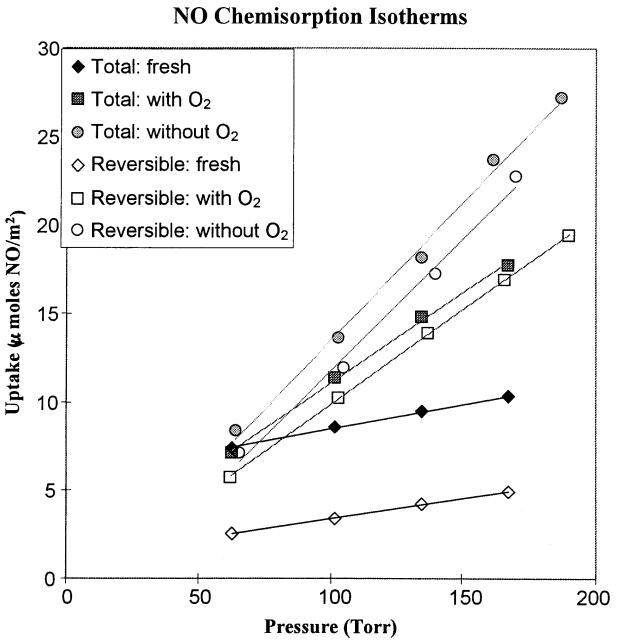

Figure 11. Effect of H_2O in feed stream on NO chemisorption at 300K after quenching. Reaction conditions: 973 K and either GHSV = 4600 h^{-1} for 10% O_2/He pretreatment (fresh) (◆, ◇) and 1.4% NO, 0.35% CH_4, 0% O_2, 2% CO_2, balance He (●, ○), or GHSV = 8300 h^{-1} for 1.4% NO, 0.35% CH_4, 1% O_2, 9% CO_2, balance He (■, □).

concentration of metal cations at the catalyst surface; additional aspects of this table have been discussed earlier [12]. Regardless, it can be seen from the table that the rate on Sr-La_2O_3 compares favorably with those for most of the other catalysts, especially considering this catalyst has a specific surface area of only 3 m^2/g *versus* values of 80–200 m^2/g for the other catalysts. The limited information available about the influence of CO_2 on NO_x reduction over oxide catalysts has been discussed elsewhere [12].

Details about the catalytic benefits of Sr-promoted La_2O_3 for NO reduction have been reported previously [4,6,30], and the most significant finding was that Sr

Table 3
Specific surface area and NO chemisorption for 4% Sr-La_2O_3 before and after reduction

	Surface area (m^2/g)	Total uptake (μmol NO/m^2)	Reversible uptake (μmol NO/m^2)	Irreversible uptake (μmol NO/m^2)
Fresh Catalyst	2.9	10.5	4.9	5.6
CO_2 study				
O_2 absent	3.0	5.5	0.69	4.8
O_2 present	2.1	8.5	3.6	4.9
H_2O study				
O_2 absent	2.1	10.1	9.1	1.0
O_2 present	2.2	7.3	6.8	0.44

Reaction conditions: 1.4% NO, 0.35% CH_4, 0 or 1.0% O_2, 0 or 9.0% CO_2, 0 or 2.0% H_2O, balance He; GHSV = 4600 h^{-1} in the absence of O_2 and 8300 h^{-1} in the presence of O_2. Uptakes were determined at 150 Torr.

appears to enhance the active site concentration at the La_2O_3 surface by creating additional oxygen vacancies; however, it was also found that Sr might promote sintering, thus decreasing the surface area. In this investigation, the effects of CO_2 and H_2O on NO reduction over this Sr-promoted catalyst were qualitatively the same as those observed with pure La_2O_3, i.e., reversible inhibition occurred, but its extent differed. At 973 K with CO_2 in the feed stream, this Sr-La_2O_3 catalyst showed a decrease in activity of 95% in the absence of O_2 and 56% in the presence of O_2 compared with respective decreases of 78 and 48% with La_2O_3. These results suggest that the Sr/LaO_3 catalyst is more sensitive than La_2O_3 to a surface oxycarbonate phase, which has been reported in an MOC study involving a SrO-promoted La_2O_3/ZnO catalyst [31]. For experiments at 973 K with H_2O in the feed, this Sr-La_2O_3 catalyst showed inhibition similar to that with La_2O_3 in the presence of O_2, 51% *versus* 46%, but in the absence of O_2, the decrease in activity was only 30% compared to 73% for La_2O_3 [12]. These results are more difficult to explain, but they may result from the following surface behavior. In the absence of O_2, H_2O adsorbs on the surface of the catalyst and dissociates *via* an interaction with atomic oxygen (O-S) on the surface. On Sr-promoted La_2O_3 this surface oxygen is more easily removed from the surface to leave an oxygen vacancy. This water-induced vacancy may explain why the Sr-promoted La_2O_3 is inhibited by H_2O to a lesser extent than pure La_2O_3; however, this still has a negative impact on overall site availability due to the competitive

Table 4
Rate comparison of NO_x reduction catalysts in the presence of O_2 and H_2O

Catalyst	Temp (K)	Reductant	(%)	H_2O (%)	NO (%)	O_2 (%)	Balance	N_2 rate (μmol/s g $\times 10^3$)	N_2 activity (μmol/s m^2 $\times 10^3$)	TOF ($s^{-1} \times 10^3$)	GHSV (h^{-1})	α [a] (%)	Reference
4% Sr-La_2O_3	923	CH_4	0.35	2.0	1.4	1.0	He	189	65	10.7	121 000	26	This study
Y_2O_3	923	CH_4	0.40	2.0	0.40	0.40	He	60	0.50	n/a [e]	30 000	12	[20]
Co/Al_2O_3	923	C_3H_6	0.06	20	0.07	3.0	N_2	75	0.46	n/a [e]	21 000	n/a [f]	[21]
4% Sr-La_2O_3	873	CH_4	0.35	2.0	1.4	1.0	He	55	19	3.1	121 000	24	This study
Co/ZSM-5	873	CH_4	0.10	0 [c]	0.10	2.0	He	67 [d]	n/a [b]	n/a [e]	40 000	14	[22]
Co-La/ZSM-5	873	CH_4	0.10	0 [c]	0.10	2.0	He	104 [d]	n/a [b]	n/a [e]	40 000	21	[22]
Ce-Ag/ZSM-5	873	CH_4	0.50	8.3	0.50	2.5	He	60 [d]	n/a [b]	2.4	7 500	31	[23]
In/ZSM-5	873	CH_4	0.10	10	0.10	10	He	15 [d]	n/a [b]	n/a [e]	30 000	n/a [f]	[24]
Co/ZSM-5	873	CH_4	0.10	2.0	0.09	2.5	He	70 [d]	n/a [b]	0.21	30 000	9	[25]
Co/ferrierite	873	CH_4	0.10	2.0	0.09	2.5	He	101 [d]	n/a [b]	0.30	30 000	14	[25]
Co/Al_2O_3	873	C_3H_6	0.06	20	0.07	3.0	N_2	98	0.60	n/a [e]	21 000	n/a [f]	[21]
Sn-Co/Al_2O_3	873	C_3H_6	0.06	20	0.07	3.0	N_2	84	0.51	n/a [e]	21 000	n/a [f]	[21]
4% Sr-La_2O_3	823	CH_4	0.35	2.0	1.4	1.0	He	15	5.2	0.86	121 000	17	This study
Co/ferrierite	823	CH_4	0.10	2.0	0.40	2.5	He	60	n/a [b]	2.7	30 000	17	[26]
Cu/Al_2O_3	823	C_3H_6	0.20	5.0	0.2	5.0	He	56	n/a [b]	0.30	15 000 [d]	14	[27]
Co/Al_2O_3	823	C_3H_6	0.06	20	0.07	3.0	N_2	75	0.46	n/a [e]	21 000	n/a [f]	[21]
Sn-Co/Al_2O_3	823	C_3H_6	0.06	20	0.07	3.0	N_2	88	0.54	n/a [e]	21 000	n/a [f]	[21]
Ag/Al_2O_3	823	C_3H_6	0.10	3.0	0.10	5.0	N_2	250	1.3	n/a [e]	40 000	25	[28]
4% Sr-La_2O_3	773	CH_4	0.35	2.0	1.4	1.0	He	6.6	2.3	0.37	121 000	28	This study
Fe/ZSM-5	773	C_4H_{10}	0.50	10	0.20	3.0	He	290	n/a [b]	0.60	42 000	14	[29]
Fe/ZSM-5	773	C_4H_{10}	0.20	20	0.20	3.0	He	990	n/a [b]	2.5	42 000	>9	[19]
Co/Al_2O_3	773	C_3H_6	0.06	20	0.07	3.0	N_2	19	0.12	n/a [e]	21 000	n/a [f]	[21]
Sn-Co/Al_2O_3	773	C_3H_6	0.06	20	0.07	3.0	N_2	75	0.46	n/a [e]	21 000	n/a [f]	[21]

[a] Defined in equation (4.1).
[b] Specific surface area not reported.
[c] Steamed for 24 h in 114 Torr of H_2O at 1073 K.
[d] Assumed catalyst density of 1 g/cm^3.
[e] Neither NO uptake nor reactive sites reported.
[f] CH_4 conversion data not reported.

adsorption of H_2O on these sites. In the presence of O_2, this possible effect due to water-induced oxygen vacancies would be balanced because of the abundance of surface oxygen via dissociative O_2 chemisorption.

Despite these differences it is reasonable to assume that the reaction mechanisms in the absence and presence of O_2 are the same as those proposed previously [30], except that CO_2 and H_2O must be included in the site balance during derivation of the rate law. A detailed sequence of elementary steps describing NO reduction by CH_4 in the absence of O_2 has been proposed previously [30], and a simplified version, which combines a number of quasi-equilibrated steps into a single reaction (equation (4)) but satisfactorily shows the kinetically significant steps, is shown below:

$$4[NO + S \overset{K_{NO}}{\rightleftharpoons} NO\text{-}S] \quad (1)$$

$$CH_4 + S \overset{K_{CH_4}}{\rightleftharpoons} CH_4\text{-}S \quad (2)$$

$$NO\text{-}S + CH_4\text{-}S \overset{k}{\longrightarrow} HNO\text{-}S + CH_3\text{-}S \text{ (rds)} \quad (3)$$

$$3NO\text{-}S + HNO\text{-}S + CH_3\text{-}S \overset{K}{\rightleftharpoons} 2H_2O\text{-}S + 2N_2 + CO_2\text{-}S + 2S \quad (4)$$

$$CO_2\text{-}S \overset{K_{CO_2}}{\rightleftharpoons} CO_2 + S \quad (5)$$

$$2[H_2O\text{-}S \overset{K_{H_2O}}{\rightleftharpoons} H_2O + S] \quad (6)$$

$$4NO + CH_4 + \longrightarrow 2N_2 + 2H_2O + CO_2 \quad (7)$$

Equation (3) represents the rate-determining step (rds), and with the following site balance for total active sites, $L = [CH_4\text{-}S] + [NO\text{-}S] + [CO_2\text{-}S] + [H_2O\text{-}S] + [S]$, the resulting rate law for N_2 formation is obtained [32]:

$$r_{N_2} = \frac{(LkK_{NO}K_{CH_4})P_{NO}P_{CH_4}}{(1 + K_{NO}P_{NO} + K_{CH_4}P_{CH_4} + K_{CO_2}P_{CO_2} + K_{H_2O}P_{H_2O})^2} \quad (8)$$

As with La_2O_3 [12], differential reactor conditions were maintained throughout the experiments in the absence of O_2, so the same optimization routine was used to determine the five fitting constants. The resulting fits to the data are quite good and are displayed as solid lines in figures 5 and 6 for CO_2 and H_2O, respectively, and the optimized values at each temperature are listed in table 5. Enthalpies and entropies of adsorption were obtained from the constants corresponding to equilibrium adsorption constants, and they are listed in table 6 along with 90% confidence limits. These values were analyzed for thermodynamic consistency and found to satisfy all criteria to be physically meaningful [33,34]. These values are very consistent with those reported for La_2O_3 under similar conditions [12]. The activation energy for the rate constant k in the rate-determining step (equation (3))

Table 5
Optimized constants for equation (8) in the absence of O_2 and equation (19) in the presence of O_2

	k'_{NO} [a]	k' [b]	K_{NO} ($Torr^{-1}$)	K_{CH_4} ($Torr^{-1}$)	K_{O_2} ($Torr^{-1}$)	K_{CO_2} ($Torr^{-1}$)	K_{H_2O} ($Torr^{-1}$)
CO_2 study							
O_2 absent							
973 K	0.17	–	0.67	8.3	–	0.085	–
960 K	0.35	–	2.0	9.9	–	0.15	–
948 K	0.31	–	1.5	12	–	0.13	–
923 K	0.50	–	2.5	20	–	0.21	–
O_2 present							
923 K	0.020	0.71	0.055	0.51	1.2	0.0075	–
908 K	0.014	1.4	0.093	0.41	0.88	0.0097	–
893 K	0.027	2.5	0.13	0.48	3.6	0.013	–
873 K	0.029	1.7	0.14	0.97	4.7	0.020	–
H_2O study							
O_2 absent							
973 K	0.0086	–	–	0.40	–	–	0.020
948 K	0.0061	–	–	0.41	–	–	0.026
923 K	0.0057	–	–	0.53	–	–	0.041
898 K	0.010	–	–	1.0	–	–	0.085
O_2 present							
923 K	0.79	45	1.2	0.057	56	–	0.29
908 K	0.87	86	1.3	0.064	67	–	0.67
893 K	1.0	180	1.7	0.084	180	–	0.45
893 K	1.7	310	3.3	0.11	290	–	1.4

[a] Units for k' are μmol $N_2(s\,m^2\,Torr^2)^{-1}$ in the absence of O_2 and μmol $N_2(s\,m^2\,Torr^{2.5})^{-1}$ in the presence of O_2.
[b] Units for k'_{com} are μmol CH_4 $(s\,m^2\,Torr^2)^{-1}$.

Table 6
Enthalpies and entropies of adsorption [a] obtained from the parameters in table 5 for the feed-stream components. Comparison with earlier results in the absence of O_2 and excess CO_2 and H_2O is provided

	NO	CH_4	O_2	CO_2	H_2O
Huang *et al.* [5]					
Absence of O_2					
ΔH^o_{ad} (kcal/mol)	−28	−20	–	–	–
S^o_{ad} (cal/mol K)	−23	−9	–	–	–
CO_2 study					
Absence of O_2					
ΔH^o_{ad} (kcal/mol)	-38 ± 20	-31 ± 6	–	-29 ± 10	–
S^o_{ad} (cal/mol K)	-26 ± 20	-15 ± 6	–	-21 ± 10	–
Presence of O_2					
ΔH^o_{ad} (kcal/mol)	-28 ± 10	-21 ± 13	-54 ± 20	-32 ± 4	–
S^o_{ad} (cal/mol K)	-23 ± 10	-12 ± 13	-45 ± 20	-31 ± 4	–
H_2O Study					
Absence of O_2					
ΔH^o_{ad} (kcal/mol)	–	-21 ± 7	–	–	-33 ± 5
S^o_{ad} (cal/mol K)	–	-11 ± 7	–	–	-29 ± 5
Presence of O_2					
ΔH^o_{ad} (kcal/mol)	-33 ± 7	-22 ± 7	-56 ± 11	–	-44 ± 20
S^o_{ad} (cal/mol K)	-22 ± 7	-17 ± 7	-40 ± 11	–	-36 ± 20

[a] With 90% confidence limits.

was 35 ± 6 kcal/mole with CO_2 in the feed, but it could not be determined in the study with H_2O because the $K_{NO}P_{NO}$ term in the partial pressure studies was too small to analyze.

As with La_2O_3 [12], both the chemistry and the data analysis become much more complex when O_2 is added to the feed because Sr-promoted La_2O_3 also catalyzes the direct oxidation of CH_4 with O_2. Consequently, differential conversions of all components could not be maintained under all reaction conditions, even though NO conversion was always less than 10%, because total methane and oxygen conversions sometimes approached 50% or more. Due to this parallel combustion reaction, analyses of rate data were conducted assuming integral reactor behavior so that accurate concentration profiles throughout the reactor could be determined and appropriate modeling of both the NO reduction and CH_4 combustion reactions could be conducted [32]. The latter reaction has been modeled and discussed elsewhere [13].

Based on the similarity of behavior between $Sr\text{-}La_2O_3$ and La_2O_3, it is reasonable to assume that the surface chemistry is the same and the sequence of elementary steps proposed earlier is still applicable [12,30]. The abbreviated reaction mechanism, which again shows the kinetically significant steps (equations (9)–(13)) and combines a number of quasi-equilibrated steps into equation (14), is given below:

$$4[NO + S \overset{K_{NO}}{\rightleftharpoons} NO\text{-}S] \quad (9)$$

$$2[CH_4 + S \overset{K_{CH_4}}{\rightleftharpoons} CH_4\text{-}S] \quad (10)$$

$$2[O_2 + 2S \overset{K_{O_2}}{\rightleftharpoons} 2O\text{-}S] \quad (11)$$

$$3[NO\text{-}S + O\text{-}S \overset{K_{NO_2}}{\rightleftharpoons} NO_2\text{-}S + S] \quad (12)$$

$$2[NO_2\text{-}S + CH_4\text{-}S \overset{k}{\longrightarrow} HNO_2\text{-}S + CH_3\text{-}S] \text{ (rds)} \quad (13)$$

$$2HNO_2\text{-}S + 2CH_3\text{-}S + NO\text{-}S + NO_2\text{-}S + O\text{-}S \overset{K}{\rightleftharpoons} 2CO_2\text{-}S + 4H_2O\text{-}S + 2N_2 \quad (14)$$

$$2[CO_2\text{-}S \overset{K_{CO_2}}{\rightleftharpoons} CO_2 + S] \quad (15)$$

$$4[H_2O\text{-}S \overset{K_{H_2O}}{\rightleftharpoons} H_2O + S] \quad (16)$$

$$4NO + 2CH_4 + 2O_2 \longrightarrow 2N_2 + 4H_2O + 2CO_2 \quad (17)$$

With equation (13) as the rds and assuming CH_4-S, NO-S, O-S, CO_2-S and H_2O-S to be the predominant surface species in the site balance, the derived rate expression for N_2 formation becomes [32]:

$$r_{N_2} = \frac{(LkK_{NO_2}K_{NO}K_{CH_4}K_{O_2}^{0.5})P_{NO}P_{CH_4}P_{O_2}^{0.5}}{(1 + K_{NO}P_{NO} + K_{CH_4} + P_{CH_4} + K_{CO_2}P_{CO_2} + K_{H_2O}P_{H_2O} + K_{O_2}^{0.5}P_{O_2}^{0.5})^2}. \quad (18)$$

This expression relates directly to CH_4 disappearance due to NO reduction based on the stoichiometry in equation (17), i.e., $r_{N_2} = (r_{CH_4})_{NO}$ because $d[N_2]/dt = -d[CH_4]/dt$. This rate expression must then be combined with that for CH_4 disappearance due only to combustion with O_2 [13] to obtain a rate equation for

total methane disappearance:

$$(r_{CH_4})_T = \frac{k'_{com} P_{CH_4} P_{O_2}^{0.5} + k'_{NO} P_{NO} P_{CH_4} P_{O_2}^{0.5}}{(1 + K_{NO} P_{NO} + K_{CH_4} P_{CH_4} + K_{O_2}^{0.5} P_{O_2}^{0.5} + K_{CO_2} P_{CO_2} + K_{H_2O} P_{H_2O})^2} \quad (19)$$

where $k'_{com} = LK_{CH_4}(K_{O_2})^{0.5}$ and $k'_{NO} = LK_{NO_2} \times K_{NO} K_{CH_4}(K_{O_2})^{0.5}$. This expression is then employed in the design equation for an integral reactor by relating the partial pressure of each component to P_{CH_4} *via* the appropriate stoichiometry [13,32]. An optimization procedure described elsewhere was used to optimize this complex rate expression [13], and the ability of this model to fit the data is displayed as solid lines in figure 7 for CO_2 in the feed and in figure 8 for H_2O in the feed. The fitting constants from the optimized expressions are listed in table 5, and the thermodynamic parameters obtained from these equilibrium adsorption constants are in Table 6. Due to the inclusion of K_{NO_2} in the lumped rate constant, it was not possible to determine the activation energy associated with the rds given in equation (13). The thermodynamic values determined in the presence of O_2 are again quite similar to those from other studies, and the enthalpies for CH_4 adsorption, in particular, show very good agreement, which implies that the interaction of CH_4 and the other adsorbates with the surface is relatively independent of the concentration of O_2, H_2O or CO_2. Similar to the La_2O_3 study in the absence of O_2, a very low surface concentration of adsorbed NO is indicated by the results with H_2O, but no O_2, in the feed. Because of the consistency between these and previous results, it is still proposed that H_2O competes with NO for O-S groups, which have been associated with enhanced NO adsorption on La_2O_3 [35,36].

Xie *et al*. [37] have also studied NO reduction with CH_4 over a 1% Sr/La_2O_3 catalyst and they also found that O_2 enhanced the rate of NO reduction. In addition, using an ESR technique they identified low concentrations of gas-phase methyl radicals at low pressures near 500 mTorr and above 800 K. In a subsequent study of this reaction over Ba/MgO catalysts, they also observed a rate inhibition due to CO_2 [38]. In both cases, no complete catalytic cycle was provided and no kinetic rate expression was derived, but the authors have suggested that gas-phase methyl radicals are responsible for NO reduction in the presence of O_2, but probably not in the absence of O_2 [38,39]. We do not disallow the possibility of gas-phase reactions involving methyl radicals, but it is our belief that the *predominant* reaction pathway in these porous catalysts involves methyl radicals and NO adsorbed on the surface. This has allowed us to model the reaction *via* a Langmuir–Hinshelwood model, to readily include the roles of CO_2 and H_2O and to fit the data well, to address CH_4 partial pressure dependencies that are far less than unity, and to obtain thermodynamic parameters that are quite consistent among La_2O_3, Sr/La_2O_3 and La_2O_3/Al_2O_3 catalyst systems. Regardless, future studies are needed to clearly delineate the homogeneous and heterogeneous contributions to the overall rate.

As in the study with La_2O_3 [12], it was difficult to reach quantitative conclusions about all the NO chemisorption experiments. The chemisorption results in figure 11 for the fresh catalyst (from the same experiment) show well-behaved adsorption behavior with the total and reversible uptakes having similar slopes, which is characteristic of equilibrated adsorption. The oxycarbonate catalyst, $La_2O_2CO_3$, exhibited significantly different behavior, especially after use in the absence of O_2. While the total and reversible isotherms diverge moderately after use in the presence of O_2, the total and irreversible uptakes are only moderately less than those for the fresh catalyst; however, after conducting the reaction in the absence of O_2, not only do the isotherms show marked divergence, but the total uptake is also less than the reversible uptake of the fresh catalyst. This observation may help explain why the activity decreased by ~95% in the absence of O_2 and suggests the following behavior with respect to CO_2 and Sr-promoted La_2O_3. The divergence in the isotherms for total and reversible chemisorption following reaction conditions with CO_2 implies that NO adsorption is not equilibrated. If so, this unequilibrated adsorption is most likely due to an oxycarbonate phase that has been shown to desorb CO_2 in the presence of NO *via* a surface reaction [15]. From the kinetic experiments combined with the XRD analysis in this study and elsewhere [12], it is apparent that the presence of O_2 facilitates decomposition of the oxycarbonate phase. This may lead to a reduced concentration of surface carbonate species compared with reaction conditions without O_2, and this might explain the similarity of the NO uptake with respect to the fresh catalyst. NO uptakes following reaction conditions with H_2O in the feed exhibited different behavior as well. The H_2O-exposed catalysts demonstrated steeper slopes for both total and reversible isotherms; in addition, the total and reversible slopes were virtually identical either in the presence or absence of O_2, and they indicated relatively low uptakes. These results show very low irreversible uptakes of NO and suggest that H_2O occupies the sites responsible for strong (irreversible) adsorption.

5. Summary

In general, the influence of CO_2 and H_2O on the activity of 4% $Sr\text{-}La_2O_3$ mimics that observed with pure La_2O_3 and reversible rate inhibition is observed, with the former catalyst being slightly more susceptible to CO_2 inhibition, but less susceptible to inhibition by H_2O, than La_2O_3. The mechanism proposed to describe NO reduction by CH_4 on La_2O_3 is applicable to this

study as well, and the rate law in the absence of O_2 is

$$r_{N_2} = \frac{(LkK_{NO}K_{CH_4})P_{NO}P_{CH_4}}{(1 + K_{NO}P_{NO} + K_{CH_4}P_{CH_4} + K_{CO_2}P_{CO_2} + K_{H_2O}P_{H_2O})^2},$$

which yields a good fit to the experimental data and gives optimized equilibrium adsorption constants that demonstrate thermodynamic consistency. In the presence of O_2, the nondifferential changes in reactant concentrations through the reactor bed were accounted for by simultaneously considering both CH_4 combustion and CH_4 reduction of NO, which provided the following rate law for total CH_4 disappearance:

$$(r_{CH_4})_T = \frac{k'_{com}P_{CH_4}P_{O_2}^{0.5} + k'_{NO}P_{NO}P_{CH_4}P_{O_2}^{0.5}}{(1 + K_{NO}P_{NO} + K_{CH_4}P_{CH_4} + K_{O_2}^{0.5}P_{O_2}^{0.5} + K_{CO_2}P_{CO_2} + K_{H_2O}P_{H_2O})^2}.$$

The second term of this expression represents N_2 formation, and it again gave meaningful fits to the experimental data and yielded thermodynamically consistent rate constants. The entropy and enthalpy of adsorption for each measurable component were consistent with values reported for other La_2O_3-based catalysts.

Acknowledgment

This study was supported by the National Science Foundation under Grant CTS-9633752.

References

[1] J.M. DeBoy and R.F. Hicks, J. Chem. Soc., Chem. Commun. (1988) 982.
[2] J.M. DeBoy and R.F. Hicks, Ind. Eng. Chem. Res. 27 (1988) 1577.
[3] J.M. DeBoy and R.F. Hicks, J. Catal. 113 (1988) 517.
[4] X. Zhang, A.B. Walters and M.A. Vannice, Appl. Catal B 7 (1996) 321.
[5] S.-J. Huang, A.B. Walters and M.A. Vannice, Appl. Catal. B 17 (1998) 183.
[6] S.-J. Huang, A.B. Walters and M.A. Vannice, J. Catal. 173 (1998) 229.
[7] Z. Kalenik and E.E. Wolf, Catal. Lett. 9 (1991) 441.
[8] S.J. Conway, J.A. Greig and G.M. Thomas, Appl. Catal. A 86 (1992) 199.
[9] A.G. Anshits, E.N. Voskresenykaya and E.V. Kondratenko, Catal. Today 24 (1995) 217.
[10] T. Le Van, M. Che, M. Kermarec, C. Louis and J.M. Tatibouet, Catal. Lett. 6 (1990) 395.
[11] H. Piao, Y.L. Bi and K.J. Zhen, Chem. Res. Chinese. Univ. 13 (1997) 39.
[12] T.J. Toops, A.B. Walters and M.A. Vannice, Appl. Catal. B, In press.
[13] T.J. Toops, A.B. Walters and M.A. Vannice, Appl. Catal. A, In press.
[14] T.J. Toops, A.B. Walters and M.A. Vannice, Catal. Lett. 64 (2000) 65.
[15] B. Klingenberg and M.A. Vannice, Chem Mater. 8 (1996) 2755.
[16] M.P. Rosynek and D.T. Magnuson, J. Catal. 46 (1977) 402.
[17] K.C. Khara, H.J. Robota and D.J. Liu, Appl. Catal. B 2 (1993) 225.
[18] J.Y. Yan, G.-D. Lei, W.M.H. Sachtler and H.H. Kung, J. Catal. 141 (1996) 161.
[19] X. Feng and W.K. Hall, J. Catal. 166 (1997) 368.
[20] M.D. Fokema and J.Y. Ying, Appl. Catal. B 18 (1998) 71.
[21] L. Chen, T. Horiuchi and T. Mori, Catal. Lett. 72(1–2) (2001) 71.
[22] P. Budi and R. Howe, Catal. Today 38 (1997) 175.
[23] Z. Li and M. Flytzani-Stephanopolous, Appl. Catal. B 22 (1999) 35.
[24] E. Kikuchi, M. Ogura, N. Aratani, Y. Sugiura, S. Hiromoto and K. Yogo, in: *Environmental Catalysis*, eds. G. Centi, S. Perathoner, C. Christani and P. Forzatti, Rome, Italy, 1995, p. 27.
[25] Y. Li and J.N. Armor, Appl. Catal. B 5 (1995) L257.
[26] Y. Li and J.N. Armor, J. Catal. 150 (1994) 376.
[27] E. A. Efthimidias, G.D. Lionta, S.C. Christoforou and I.A. Vasalos, Catal. Today 40 (1998) 15.
[28] A. Martinez-Arias, M. Fernandez-Garcia, A. Iglesias-Juez, J.A. Anderson, J.C. Conesa and J. Soria, Appl. Catal. B 28 (2000) 29.
[29] H.-Y. Chen and W.M.H. Sachtler, Catal. Today 42 (1998) 73.
[30] M.A. Vannice, A.B. Walters and X. Zhang, J. Catal. 159 (1996) 119.
[31] Y.D. Xu, L. Yu and X.X. Guo, Appl. Catal. A 164(1–2) (1997) 47.
[32] T.J. Toops, Ph.D. Thesis, The Pennsylvania State University, 2001.
[33] M. Boudart, AIChE J. 18 (1972) 465.
[34] M.A. Vannice, S.H. Hyun. B. Kalpakci and W.C. Liauh, J. Catal. 56 (1979) 358.
[35] S.-J. Huang, A.B. Walters and M.A. Vannice, J. Catal. 192 (2000) 29.
[36] S.-J. Huang, A.B. Walters and M.A. Vannice, Catal. Lett. 64 (2000) 77.
[37] S. Xie, T.H. Ballinger, M.P. Rosynek and J.H. Lunsford, 11th International Congress on Catalysis, in: *Studies in Surface Science and Catalysis*, Vol. 101, eds. J.W. Hightower, W.N. Delgass, E. Iglesia and A.T. Bell (Elsevier, Amsterdam, 1996), p. 711.
[38] S. Xie, M.P. Rosynek and J.H. Lunsford, J. Catal. 188 (1999) 32.
[39] S. Xie, M.P. Rosynck and J.H. Lunsford, Catal. Lett. 43 (1997) 1.